

Observation of unconventional superconductivity in new layered superconductor $\text{Ta}_4\text{Pd}_3\text{Te}_{16}$

J. Pan¹, W. H. Jiao², X. C. Hong¹, Z. Zhang¹, L. P. He¹, P. L. Cai¹, J. Zhang¹, G. H. Cao² & S. Y. Li^{1*}

¹*State Key Laboratory of Surface Physics, Department of Physics, and Laboratory of Advanced Materials, Fudan University, Shanghai 200433, China*

²*Department of Physics, Zhejiang University, Hangzhou 310027, China*

*: *Correspondence should be addressed to: shiyan_li@fudan.edu.cn*

Finding unconventional superconductors and understanding their superconducting mechanism is one of the main themes in condensed matter physics. Unconventional superconductivity usually resides in quasi-two-dimensional compounds, such as the high-temperature cuprate and iron-based superconductors. When further reducing the dimensionality, namely in quasi-one-dimensional (Q1D) superconductors, it is much less clear whether the pairing symmetry and mechanism are unconventional. Here we measure the low-temperature thermal conductivity of a new layered superconductor with Q1D characteristics, the ternary telluride $\text{Ta}_4\text{Pd}_3\text{Te}_{16}$ with transition temperature $T_c = 4.3$ K. The significant residual linear term of thermal conductivity in zero magnetic field and its rapid field dependence clearly reveal the presence of nodes in the superconducting gap. By measuring resistivity under pressure, we discover a superconducting dome in the temperature-pressure phase diagram. The existence of gap nodes and superconducting dome strongly indicates unconventional superconductivity in $\text{Ta}_4\text{Pd}_3\text{Te}_{16}$. Our finding may shed new light on the pairing mechanism of Q1D superconductors.

Superconductivity is a fundamental quantum ground state in condensed matters. While conventional phonon-mediated s-wave superconductivity has been well understood for decades, the unconventional superconductivity remains a big challenge in recent years (1). The term “unconventional” firstly means the superconducting pairing mechanism is not phonon-mediated. This usually manifests as a superconducting dome neighbouring a magnetic order in the phase diagram, and spin fluctuations are considered as the major pairing glue (1). Secondly, the term “unconventional” means the wave function of Cooper pairs is not s-wave. Symmetry imposed nodes (gap zeros) are often observed, such as in d-wave cuprate superconductors and heavy-fermion superconductor CeCoIn₅ (2,3), and in p-wave superconductor Sr₂RuO₄ (4). Note that the iron-based superconductors may be exceptions, with the form of s_±-wave (5). The superconducting gap symmetry and structure may provide important clue to the underlying pairing mechanism.

One more feature of unconventional superconductors is their low dimensionality. For example, many unconventional superconductors are quasi-two-dimensional (Q2D), such as cuprate and iron-based superconductors, CeCoIn₅, Sr₂RuO₄, and organic superconductors κ-(BEDT-TTF)₂X (1). In quasi-one-dimensional (Q1D) superconductors, represented by the organic compounds (TMTSF)₂X (X = PF₆, ClO₄) (6, 7), it is still very controversial whether the superconductivity is unconventional (8). The main reason for the controversy is that their superconducting states are inconvenient for many experimental investigations, due to very low T_c , requiring pressure, and additional anion ordering (8).

Recently, the ternary telluride Ta₄Pd₃Te₁₆ was found to be a new layered superconductor with Q1D characteristics (9). The T_c is about 4.5 K at ambient pressure. It has relatively flat Ta–Pd–Te layers in the (-103) plane, which contains PdTe₂, TaTe₃, and Ta₂Te₄ chains along the crystallographic b axis, as illustrated in Fig. 1. Here we

present the low-temperature thermal conductivity measurements of Ta₄Pd₃Te₁₆ single crystal down to 80 mK, which clearly demonstrates that there are nodes in the superconducting gap. Furthermore, a superconducting dome in the temperature-pressure phase diagram is revealed by resistivity measurements. These results suggest unconventional superconductivity in Ta₄Pd₃Te₁₆. Due to its Q1D characteristics, our finding may help to understand the pairing mechanism of Q1D superconductors.

Figure 2A shows the low-temperature dc magnetization of Ta₄Pd₃Te₁₆ single crystal. With zero-field-cooling process, a sharp diamagnetic superconducting transition is observed at $T_c \approx 4.3$ K. In Fig. 2B, the resistivity of Ta₄Pd₃Te₁₆ single crystal in zero field is plotted. The resistivity decreases smoothly from room temperature to T_c , without showing any anomaly due to additional ordering. Fitting the data between 7 and 25 K to $\rho(T) = \rho_0 + AT^n$ gives residual resistivity $\rho_0 = 3.96 \mu\Omega \text{ cm}$ and $n = 2.26$. This value of n is reasonable for a Q1D metal, in which the electron-electron umklapp process results in $2 \leq n \leq 3$ (10). The $T_c = 4.3$ K is defined by $\rho = 0$, which agrees well with the magnetization measurement.

To determine the upper critical field $H_{c2}(0)$ of Ta₄Pd₃Te₁₆, we measure the resistivity down to 0.3 K in various magnetic fields. Figure 2C shows the low-temperature resistivity in fields up to 3 T. The temperature dependence of H_{c2} , defined by $\rho = 0$ on the resistivity curves in Fig. 2C, is plotted in Fig. 2D. The dashed line is a guide to the eye, which points to $H_{c2}(0) \approx 2.9$ T. The inset shows the field dependence of ρ_0 , which manifests positive magnetoresistance, with $\rho_0(2\text{T}) = 4.54 \mu\Omega \text{ cm}$.

Low-temperature heat transport is an established bulk technique to probe the superconducting gap structure (11). The thermal conductivity results of Ta₄Pd₃Te₁₆ single crystal are presented in Fig. 3. Figure 3A shows the temperature dependence of thermal conductivity in $H = 0, 0.2, 0.3, 0.5, 1, 1.5,$ and 2 T magnetic fields, plotted as

κ/T vs T . All the curves are roughly linear, as observed in nodal superconductor KFe_2As_2 single crystal with comparable ρ_0 (12). Therefore we fit the data to $\kappa/T = a + bT^{\alpha-1}$ with α fixed to 2. The two terms aT and bT^α represent contributions from electrons and phonons, respectively. Below we only focus on the electronic term.

In zero field, the fitting gives a residual linear term with coefficient $\kappa_0/T \equiv a = 1.96 \pm 0.02 \text{ mW K}^{-2} \text{ cm}^{-1}$. This value is more than 30% of the normal-state Wiedemann-Franz law expectation $\kappa_{N0}/T = L_0/\rho_0(0T) = 6.19 \text{ mW K}^{-2} \text{ cm}^{-1}$, where L_0 is the Lorenz number $2.45 \times 10^{-8} \text{ W } \Omega \text{ K}^{-2}$ and $\rho_0(0T) = 3.96 \text{ } \mu\Omega \text{ cm}$. In nodeless superconductors, there are no fermionic quasiparticles to conduct heat as $T \rightarrow 0$, since all electrons become Cooper pairs. Therefore there is no residual linear term of κ , i.e., $\kappa_0/T = 0$. However, for unconventional superconductors with nodes in the superconducting gap, the nodal quasiparticles will contribute a finite κ_0/T in zero field (11). For example, $\kappa_0/T = 1.41 \text{ mW K}^{-2} \text{ cm}^{-1}$ for the overdoped d -wave cuprate superconductor $\text{Tl}_2\text{Ba}_2\text{CuO}_{6+\delta}$ (Tl-2201), which is about 36% of its κ_{N0}/T (13), and $\kappa_0/T = 17 \text{ mW K}^{-2} \text{ cm}^{-1}$ for the p -wave superconductor Sr_2RuO_4 , which is about 9% of its κ_{N0}/T (14). Therefore, the significant κ_0/T of $\text{Ta}_4\text{Pd}_3\text{Te}_{16}$ in zero field is strong evidence for the presence of nodes in the superconducting gap (11).

From Fig. 3A, a small field $H = 0.2 \text{ T}$ has significantly increased the κ/T . Above $H = 1 \text{ T}$, κ/T tends to saturate. For $H = 1.5$ and 2 T , $\kappa_0/T = 5.07 \pm 0.05$ and $5.16 \pm 0.04 \text{ mW K}^{-2} \text{ cm}^{-1}$ were obtained from the fittings, respectively. The value for $H = 2 \text{ T}$ roughly meets the normal-state Wiedemann-Franz law expectation $L_0/\rho_0(2T) = 5.40 \text{ mW K}^{-2} \text{ cm}^{-1}$. We take $H = 2 \text{ T}$ as the bulk $H_{c2}(0)$ of $\text{Ta}_4\text{Pd}_3\text{Te}_{16}$. To choose a slightly different bulk $H_{c2}(0)$ does not affect our discussions of the field dependence of κ_0/T below.

In Fig. 3B, the normalized κ_0/T of $\text{Ta}_4\text{Pd}_3\text{Te}_{16}$ is plotted as a function of H/H_{c2} , together with the clean s-wave superconductor Nb (15), the dirty s-wave

superconducting alloy InBi (16), the multi-band s-wave superconductor NbSe₂ (17), and the overdoped d-wave cuprate superconductor Tl-2201 (13). For Ta₄Pd₃Te₁₆, the field dependence of κ_0/T clearly mimics the behaviour of Tl-2201. This rapid increase of κ_0/T in magnetic field results from the Volovik effect of nodal quasiparticles, and provides further evidence for nodes in the superconducting gap (11). To our knowledge, so far all nodal superconductors have unconventional pairing mechanism (1). In this regard, the nodal gap we demonstrate from thermal conductivity results suggests unconventional superconductivity in Ta₄Pd₃Te₁₆.

To get further clue to the pairing mechanism in Ta₄Pd₃Te₁₆, we map out its temperature-pressure phase diagram by resistivity measurements under pressure. Figure 4A and 4B present the low-temperature resistivity of another Ta₄Pd₃Te₁₆ single crystal under various pressures up to 21.9 kbar. At ambient pressure, the T_c is 4.2 K. With increasing pressure, the T_c first increases sharply to 6.7 K at 3.1 kbar, enhanced by 60%. Then it decreases slowly to 1.8 K at 21.9 kbar. The pressure dependence of T_c is plotted in Fig. 4C, which shows a clear superconducting dome.

A temperature-pressure (T_c vs p) or temperature-doping (T_c vs x) superconducting dome has been commonly observed in many unconventional superconductors, including heavy-fermion superconductors, cuprate superconductors, iron-based superconductors, and Q2D organic superconductors (1). Particularly, the heavy-fermion superconductor CeCoIn₅ is non-magnetic at ambient pressure, but it also manifests a T_c vs p superconducting dome (18). An antiferromagnetic ordered state was proposed at the negative pressure side in the phase diagram of CeCoIn₅, and the unconventional superconductivity may relate to the antiferromagnetic quantum critical point (QCP) (18). Similarly, in the generalised phase diagram of Q1D compounds (TMTSF)₂X, a spin-density-wave (SDW) order lies at the negative pressure side of the non-magnetic (TMTSF)₂ClO₄, neighbouring the superconducting dome (8). There is no obvious long-

range ordered state in $\text{Ta}_4\text{Pd}_3\text{Te}_{16}$. Due to the similarities, a reasonable speculation is that there is a QCP at a small negative pressure in the phase diagram of $\text{Ta}_4\text{Pd}_3\text{Te}_{16}$, as depicted in Fig. 4D. Such a QCP very likely comes from the suppression of a magnetic order, however, we can not rule out the charge-density-wave (CDW) QCP at this stage. The ordered state may be reached by chemical substitution, i.e., a negative chemical pressure. Nevertheless, the clue we get from the observed superconducting dome is that the unconventional superconductivity in $\text{Ta}_4\text{Pd}_3\text{Te}_{16}$ may relate to some kind of quantum fluctuations.

If the Q1D characteristics play a key role in the superconductivity of $\text{Ta}_4\text{Pd}_3\text{Te}_{16}$, it may have the same pairing mechanism as those Q1D organic superconductors. However, the unconventional superconductivity in Q1D organic superconductors has not been firmly demonstrated by experiments yet. Thermal conductivity and muon-spin rotation measurements on $(\text{TMTSF})_2\text{ClO}_4$ single crystals suggested a nodeless superconducting gap (19, 20), but field-angle-resolved heat capacity measurements provided evidence of nodal superconductivity (21). While the nuclear magnetic resonance (NMR) experiments on $(\text{TMTSF})_2\text{PF}_6$ suggested spin-triplet superconductivity (22), similar experiments on $(\text{TMTSF})_2\text{ClO}_4$ gave evidence for spin-singlet pairing (23). Theoretically, it is also not clear which kind of superconducting state should exist on the disconnected Q1D Fermi surfaces near an SDW QCP (8). Various superconducting states were proposed, including nodeless spin-triplet (24), nodeless d-wave (25), and f-wave (26). From the aspect of material itself, $\text{Ta}_4\text{Pd}_3\text{Te}_{16}$ is a much better compound for experimental investigation than those organic compounds, therefore further studies of $\text{Ta}_4\text{Pd}_3\text{Te}_{16}$ may shed new light on the pairing mechanism of Q1D superconductors.

Even if the Q1D characteristics do not play the major role in the superconductivity of $\text{Ta}_4\text{Pd}_3\text{Te}_{16}$, it is still very interesting to further investigate its unconventional superconducting state. More experiments are needed to determine whether the pairing

state is spin singlet or triplet, to directly observe its nodal gap structure in momentum space, and to detect possible spin or charge fluctuations. Clarifying the pairing symmetry and mechanism of this new layered superconductor will give us new understandings of unconventional superconductivity.

References and Notes

1. M. R. Norman, *Science* **332**, 196-200 (2011).
2. C. C. Tsuei, J. R. Kirtley, *Rev. Mod. Phys.* **72**, 969-1016 (2000).
3. K. An *et al.*, *Phys. Rev. Lett.* **104**, 037002 (2010).
4. A. P. Mackenzie, Y. Maeno, *Rev. Mod. Phys.* **75**, 657-712 (2000).
5. P. J. Hirschfeld, M. M. Korshunov, I. I. Mazin, *Rep. Prog. Phys.* **74**, 124508 (2011).
6. D. Jérôme, A. Mazaud, M. Ribault, K. Bechgaard, *J. Phys. Lett.* **41**, L95-L98 (1980).
7. K. Bechgaard, K. Carneiro, M. Olsen, F. B. Rasmussen, C. S. Jacobsen, *Phys. Rev. Lett.* **46**, 852-855 (1981).
8. W. Zhang, C. A. R. Sá de Melo, *Adv. Phys.* **56**, 545-652 (2007).
9. W. H. Jiao *et al.*, *J. Am. Chem. Soc.* **136**, 1284-1287 (2014).
10. A. Oshiyama, K. Nakao, H. Kamimura, *J. Phys. Soc. Jpn.* **45**, 1136-1146 (1978).
11. H. Shakeripour, C. Petrovic, L. Taillefer, *New J. Phys.* **11**, 055065 (2009).
12. J. K. Dong *et al.*, *Phys. Rev. Lett.* **104**, 087005 (2010).
13. C. Proust, E. Boaknin, R. W. Hill, L. Taillefer, A. P. Mackenzie, *Phys. Rev. Lett.* **89**, 147003 (2002).
14. M. Suzuki *et al.*, *Phys. Rev. Lett.* **88**, 227004 (2002).
15. J. Lowell, J. B. Sousa, *J. Low. Temp. Phys.* **3**, 65-87 (1970).

16. J. Willis, D. Ginsberg, *Phys. Rev. B* **14**, 1916-1925 (1976).
17. E. Boaknin *et al.*, *Phys. Rev. Lett.* **90**, 117003 (2003).
18. V. A. Sidorov *et al.*, *Phys. Rev. Lett.* **89**, 157004 (2002).
19. S. Belin, K. Behnia, *Phys. Rev. Lett.* **79**, 2125 (1997).
20. F. L. Pratt, T. Lancaster, S. J. Blundell, C. Baines, *Phys. Rev. Lett.* **110**, 107005 (2013).
21. S. Yonezawa *et al.*, *Phys. Rev. B* **85**, 140502 (2012).
22. I. J. Lee *et al.*, *Phys. Rev. Lett.* **88**, 017004 (2002).
23. J. Shinagawa *et al.*, *Phys. Rev. Lett.* **98**, 147002 (2007).
24. M. Kohmoto, M. Sato, *Europhys. Lett.* **56**, 736-740 (2001).
25. H. Shimahara, *Phys. Rev. B* **61**, R14936-R14939 (2000).
26. K. Kuroki, R. Arita, H. Aoki, *Phys. Rev. B* **63**, 094509 (2001).

Acknowledgements We thank X. H. Chen, J. K. Dong, and D. L. Feng for helpful discussions. This work is supported by the Ministry of Science and Technology of China (National Basic Research Program No. 2012CB821402), the Natural Science Foundation of China, Program for Professor of Special Appointment (Eastern Scholar) at Shanghai Institutions of Higher Learning.

Fig. 1. The crystal structure of Ta₄Pd₃Te₁₆. (A) A view parallel to the *ac* plane. The compound crystallizes in space group *I2/m* with a monoclinic unit cell of $a = 17.687(4)$ Å, $b = 3.735(1)$ Å, $c = 19.510(4)$ Å, and $\beta = 110.42^\circ$. The crystal structure has relatively flat Ta–Pd–Te layers in the (-103) plane. The Pd atoms are octahedrally coordinated, forming edge-sharing PdTe₂ chains along the *b* axis. (B) A three-dimensional perspective view along the *b* axis. The PdTe₂ chains are separated by TaTe₃ chains and Ta₂Te₄ double chains. Therefore, Ta₄Pd₃Te₁₆ is a layered compound with quasi-one-dimensional characteristics.

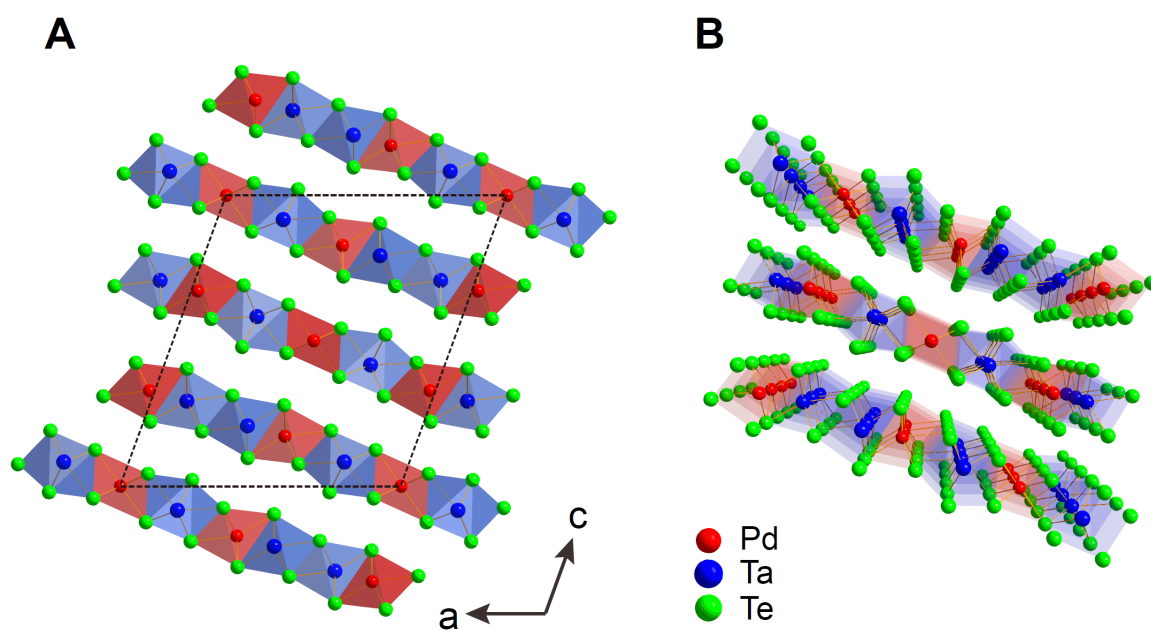


Fig. 2. (A) The dc magnetization at $H = 10$ Oe for $\text{Ta}_4\text{Pd}_3\text{Te}_{16}$ single crystal, with both zero-field-cooling (ZFC) and field-cooling (FC) processes. (B) The resistivity $\rho(T)$ along the chain direction of $\text{Ta}_4\text{Pd}_3\text{Te}_{16}$ single crystal in zero field. The blue line is a fit of the data between 7 and 25 K to $\rho(T) = \rho_0 + AT^n$, giving residual resistivity $\rho_0 = 3.96 \mu\Omega \text{ cm}$ and $n = 2.26$. (C) Low-temperature resistivity in magnetic fields up to 3 T. (D) The temperature dependence of upper critical field H_{c2} , defined by $\rho = 0$. The dashed line is a guide to the eye, which points to $H_{c2}(0) \approx 2.9$ T. The inset shows the field dependence of residual resistivity ρ_0 .

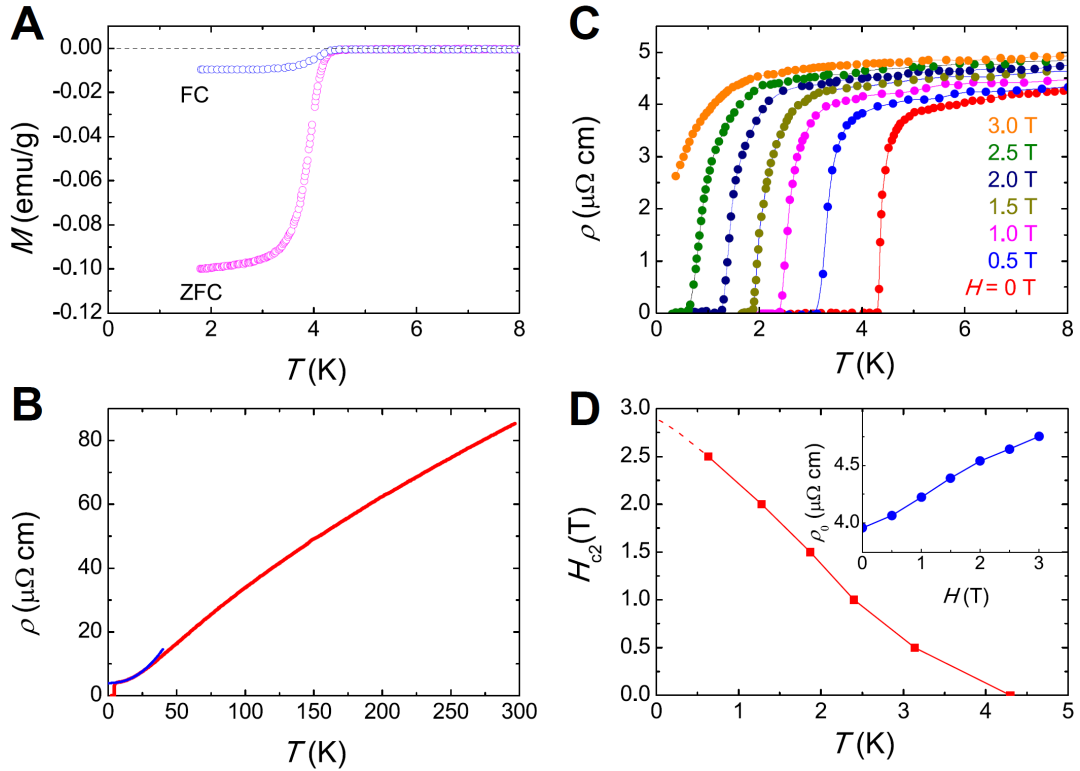


Fig. 3. (A) Low-temperature thermal conductivity of $\text{Ta}_4\text{Pd}_3\text{Te}_{16}$ in magnetic fields up to 2 T, applied perpendicular to the (-103) plane. All the curves are roughly linear. The solid lines are fits to $\kappa/T = a + bT$. The dashed line is the normal-state Wiedemann-Franz law expectation $L_0/\rho_0(2\text{T})$, with L_0 the Lorenz number $2.45 \times 10^{-8} \text{ W } \Omega \text{ K}^{-2}$ and $\rho_0(2\text{T}) = 4.54 \mu\Omega \text{ cm}$. **(B)** Normalized κ_0/T of $\text{Ta}_4\text{Pd}_3\text{Te}_{16}$ as a function of H/H_{c2} . Similar data of the clean s-wave superconductor Nb (15), the dirty s-wave superconducting alloy InBi (16), the multi-band s-wave superconductor NbSe₂ (17), and an overdoped d-wave superconductor Tl-2201 (13) are also shown for comparison. The normalized $\kappa_0(H)/T$ of $\text{Ta}_4\text{Pd}_3\text{Te}_{16}$ clearly mimics that of Tl-2201.

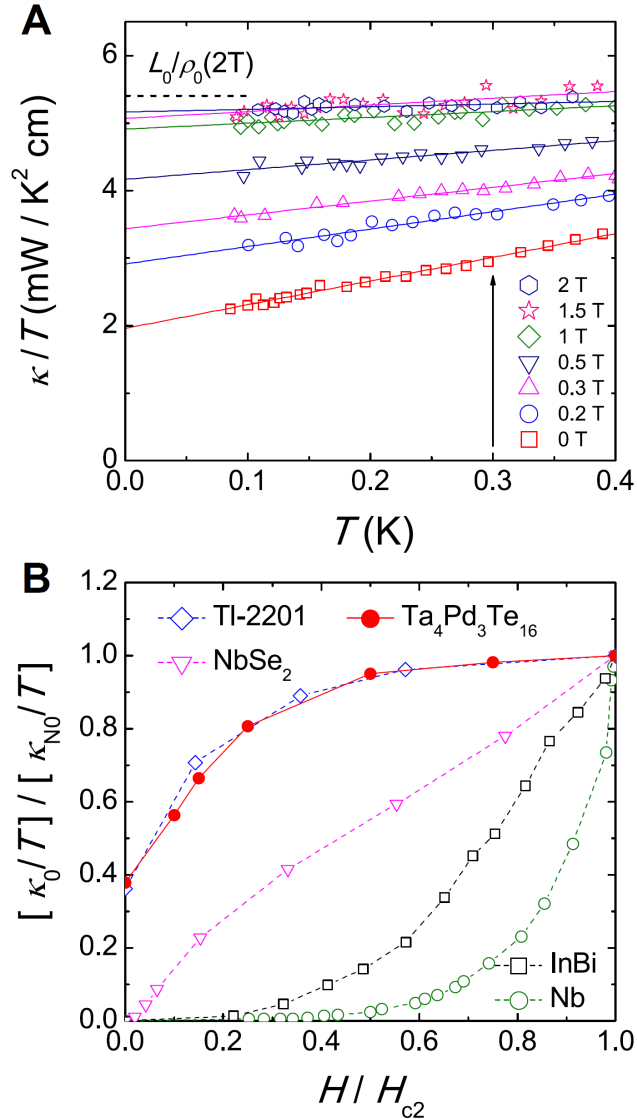
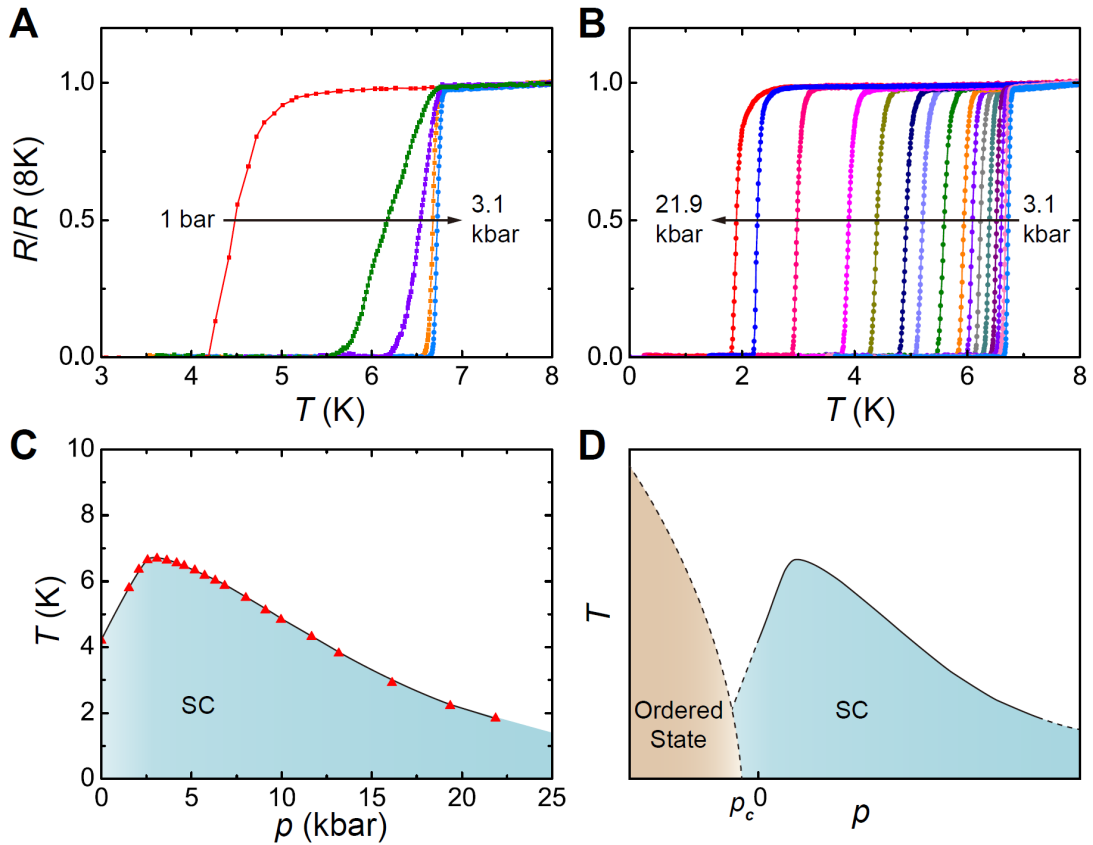


Fig. 4. Temperature-pressure phase diagram of Ta₄Pd₃Te₁₆. (A) and (B) Low-temperature resistivity of another Ta₄Pd₃Te₁₆ single crystal under various pressures up to 21.9 kbar. (C) The pressure dependent T_c , defined by $\rho = 0$. There is a clear superconducting dome, with maximum $T_c = 6.7$ K at optimal pressure $p = 3.1$ kbar. (D) The schematic phase diagram of Ta₄Pd₃Te₁₆. A QCP of an ordered state at a small negative pressure p_c is proposed. Such a QCP very likely comes from the suppression of a magnetic order, however a charge-density-wave (CDW) QCP can not be ruled out at this stage.



Supporting Online Materials

Materials and methods:

Single crystals of $\text{Ta}_3\text{Pd}_4\text{Te}_{16}$ were grown by a self-flux method [S1]. The shiny crystals in flattened needle shapes have a typical dimension of $2.5 \times 0.25 \times 0.1 \text{ mm}^3$, with the longest edge along the chain direction. The dc magnetization measurements were performed in a SQUID (MPMS, Quantum Design), with an applied field of $H = 10 \text{ Oe}$ parallel to the chain direction. Four contacts were made directly on the sample surfaces with silver paint, which were used for both resistivity and thermal conductivity measurements along the chain direction at ambient pressure. The resistivity was measured in a ^4He cryostat from 300 K to 2 K, and a ^3He cryostat down to 0.3 K. The thermal conductivity was measured in a dilution refrigerator, using a standard four-wire steady-state method with two RuO_2 chip thermometers, calibrated in situ against a reference RuO_2 thermometer. Magnetic fields were applied perpendicular to the (-103) plane. To ensure a homogeneous field distribution in the sample, all fields were applied at temperature above T_c for transport measurements. For resistivity measurements under pressure, the contacts were made with silver epoxy. Samples were pressurized in a piston-cylinder clamp cell made of Be-Cu alloy, with pressure media Daphne oil. The pressure inside the cell was determined from the T_c of a tin wire.

References:

S1. W. H. Jiao *et al.*, *J. Am. Chem. Soc.* **136**, 1284–1287 (2014).